Remote Sensing of Environment 209 (2018) 240–252

Contents lists available at ScienceDirect

Remote Sensing of Environment

journal homepage: www.elsevier.com/locate/rse

Snow cover and snow albedo changes in the central Andes of Chile and Argentina from daily MODIS observations (2000–2016)

Jeppe K. Malmros[a,*], Sebastian H. Mernild[b,c,d], Ryan Wilson[e], Torbern Tagesson[a], Rasmus Fensholt[a]

[a] Department of Geosciences and Natural Resource Management, University of Copenhagen, Copenhagen, Denmark
[b] Nansen Environmental and Remote Sensing Center, Bergen, Norway
[c] Direction of Antarctic and Sub-Antarctic Programs, Universidad de Magallanes, Punta Arenas, Chile
[d] Faculty of Engineering and Science, Western Norway University of Applied Sciences, Sogndal, Norway
[e] Department of Geography and Earth Sciences, Aberystwyth University, Aberystwyth, UK

ARTICLE INFO

Keywords:
Andes
Argentina
Chile
Climate change
ENSO
MOD10A1
MODIS
Snow albedo
Snow cover extent
Time series analysis

ABSTRACT

The variables of snow cover extent (SCE), snow cover duration (SCD), and snow albedo (SAL) are primary factors determining the surface energy balance and hydrological response of the cryosphere, influencing snow pack and glacier mass-balance, melt, and runoff conditions. This study examines spatiotemporal patterns and trends in SCE, SCD, and SAL (2000–2016; 16 years) for central Chilean and Argentinean Andes using the MODIS MOD10A1 C6 daily snow product. Observed changes in these variables are analyzed in relation to climatic variability by using ground truth observations (meteorological data from the El Yeso Embalse and Valle Nevado weather stations) and the Multivariate El Niño index (MEI) data. We identified significant downward trends in both SCE and SAL, especially during the onset and offset of snow seasons. SCE and SAL showed high inter-annual variability which correlate significantly with MEI applied with a one-month time-lag. SCE and SCD decreased by an average of ~13 ± 2% and 43 ± 20 days respectively, over the study period. Analysis of spatial pattern of SCE indicates a slightly greater reduction on the eastern side (~14 ± 2%) of the Andes Cordillera compared to the western side (~12 ± 3%). The downward SCE, SAL, and SCD trends identified in this study are likely to have adverse impacts on downstream water resource availability to agricultural and densely populated regions in central Chile and Argentina.

1. Introduction

Snow in the semi-arid mountain regions of the central Andes of Chile and Argentina provides important water resources to > 10 million people and is of major importance for agriculture in this area (Masiokas et al., 2006). Moreover, snow constitutes a key seasonal component in the surface energy and hydrosphere budgets, reflecting incoming solar shortwave radiation (e.g., Konzelmann and Ohmura, 1995). Hydrological balance in the cryosphere is highly influenced by the amount of snow precipitation and the spatiotemporal variability of seasonal snow cover extent (SCE). The combined variability of snow precipitation, SCE, and snow cover duration (SCD) directly influences river-runoff variabilities and glacier surface-mass balance conditions (Ragettli et al., 2016; Wilson et al., 2016).

On high mountain glaciers, energy availability for snow and ice melt is regulated by surface albedo which is defined as the ratio of incoming solar radiation reflected by a surface (Cuffey and Paterson, 2010). Fresh snow, for example, acts as a near perfect reflector with albedo values of up to 0.98. However, snow albedo (SAL) diminishes over time as a result of snow metamorphism, decreasing to as low as 0.46 (Cuffey and Paterson, 2010). Rainfall can further enhance this natural lowering of SAL through the addition of latent energy, which can initiate melting (Benn and Evans, 2010) and cause downwasting and thinning of glaciers (Neckel et al., 2017). Snow and ice albedo can also be reduced by the surface deposition of dust and/or anthropogenic soot (Hansen and Nazarenko, 2004; Cereceda-Balic et al., 2012). In the central Andes, an additional factor which influences SAL is the seasonal formation of penitents. Often forming in areas of low humidity and high solar elevation, snow penitents can result in significant changes in the surface roughness of snow-covered terrain, which, in turn, influences SAL and sublimation conditions (Corripio and Purves, 2006).

The overall variability of SAL is influenced by a variety of factors: snow grain size, levels of contamination, solar zenith angle, cloud cover, snow metamorphism, surface roughness, age factor, and liquid

* Corresponding author at: Department of Geosciences and Natural Resource Management, University of Copenhagen, Øster Voldgade 10, 1350 Copenhagen, Denmark.
E-mail address: vwh636@alumni.ku.dk (J.K. Malmros).

https://doi.org/10.1016/j.rse.2018.02.072
Received 1 February 2017; Received in revised form 22 February 2018; Accepted 24 February 2018
Available online 19 March 2018
0034-4257/ © 2018 Elsevier Inc. All rights reserved.

water content, amongst others (Warren and Wiscombe, 1980; Mernild et al., 2015a). Since SAL is a key parameter determining the amount of energy available for surface melting snow and ice, snow-sublimation, and metamorphosis, spatiotemporal variability in SAL is important when determining snow ablation conditions (Male and Granger, 1981; Brock et al., 2000; Hock, 2005; Gardner and Sharp, 2010; Mernild et al., 2016a).

Spatiotemporal trends in SCE and SAL interpolated from point measurements often include large errors, especially in remote mountainous regions characterized by limited ground observations, localized climate conditions and complex terrain. In comparison, satellite-based remote sensing and satellite derived snow cover products provide opportune sources of large-scale SCE and SAL measurements and have been successfully used as key inputs in climate, atmospheric and hydrological models (Farr et al., 2007; Mernild et al., 2008; Vuille et al., 2008; Mernild et al., 2015a). Remote sensing systems acquiring data from the visible (VIS) to shortwave infrared (SWIR) spectrum with a high temporal resolution are well suited for monitoring SCE and SAL over large areas, providing good spatial and temporal coverage (Wiscombe and Warren, 1980; Dozier and Frew, 1981; Dubayah, 1992; Knap et al., 1999).

Several remote sensing based snow cover products are currently available, most of which apply either the normalized difference snow index (NDSI) (Hall et al., 1995), empirical relationship assumptions or spectral un-mixing models (Klein and Stroeve, 2002). Optical sensor systems, however, are unable to acquire useful information during cloudy conditions (Justice et al., 1998; Marchane et al., 2015). Therefore, frequent satellite observation revisits are essential to study changes in SCE and SAL, since surface conditions can vary rapidly and may change considerably over a few days.

To compensate for extensive cloud cover, compromises are often made by conducting satellite analysis based on composite products such as the MODIS (Moderate Resolution Imaging Spectroradiometer) 8 day snow cover MOD10A2 product (Hall et al., 2002), which can mask subtle changes in SCE and SAL over time. In order to avoid this limitation, the MODIS MOD10A1 Collection 6 (C6) dataset was used this study. MOD10A1 provides daily SCE and SAL values globally at a spatial resolution of 500 m, making it suitable for evaluating seasonal trends in SCE and SAL (Hall et al., 2002; Liang et al., 2005; Marchane et al., 2015; Hall and Riggs, 2016; Saavedra et al., 2016; Li et al., 2017a, 2017b; Huang et al., 2017; Dariane et al., 2017), snow cover phenology (Xu et al., 2017) and the relation between SCE and climate (Gurung et al., 2017; Li et al., 2017a, 2017b). Using MOD10A1 data, this study analyses spatiotemporal changes in SCE and SAL in the central Andes of Chile and Argentina by parameterizing a time series of seasonal SCE and SAL metrics at the per-pixel level. Furthermore, this study examines the large-scale influence of ENSO events on SCE and SAL as well as the more localized effect of climatic variability (utilizing meteorological data from the El Yeso Embalse (EYE) and Valle Nevado (VN) automatic weather stations (AWS)) and elevation.

2. Study area

The Andes of central Chile and Argentina (31°S and 40°S) contain some of the highest peaks of the entire Andes Cordillera, reaching altitudes above 6000 m above sea level (a.s.l.) (Fig. 1). Covering an area of ~1730 km^2, the study area chosen is located immediately west of Santiago de Chile (32°50′–34°50′S; 69°20′–70°40′W). This study area includes several river basins which supply freshwater to large downstream populations (10+ million people in Chile and 2+ million in Argentina), hydro-power stations, and agricultural lands on both sides of the cordillera (Corripio and Purves, 2006). This area of the central Andes also includes the largest glaciated areas in South America outside southern Patagonia (Saavedra et al., 2016). River runoff in this central region originates primarily from snowmelt (Masiokas et al., 2006), with snowfall contributing up to ~85% of runoff from specific catchments (Mernild et al., 2016b). The availability of snow as a freshwater resource is therefore of vital socio-economic importance in this semi dry region (Peña and Nazarala, 1987; Meza et al., 2012; Carey et al., 2017).

The intra-annual variability of precipitation in central Andes is highly influenced by the placement of an atmospheric high-pressure cell over the southeastern Pacific Ocean. This cell normally inhibits precipitation in the Austral summer (December–February) and allows for the passage of westerlies and frontal precipitation during Austral winters (June–August) (Garreaud et al., 2009). Precipitation events are usually concentrated between April and October, providing ~95% of the mean annual totals, peaking in June or July (Masiokas et al., 2016). The strength of El Niño Southern Oscillation (ENSO) influences interannual variability in precipitation, with higher/lower precipitation occurring during El Niño/La Niña events (Rutllant and Fuenzalida, 1991; Escobar et al., 1995; Leiva, 1999; Montecinos and Aceituno, 2003; Garreaud et al., 2009). During El Niño events, precipitation increases predominantly during the austral winter (Masiokas et al., 2006; McClung, 2013). While El Niño events do influence precipitation amounts, these events shows little or no significant signal in annual mass balance measurements of glaciers located in the central Andes but has been linked to the Pacific Decadal Oscillation (PDO) rather than the ENSO (Mernild et al., 2015a).

Along the central Andes, annual accumulation of snow is highest at 4000–5000 m a.s.l., where glacier accumulation zones are also present (Cornwell et al., 2016; Mernild et al., 2016b; Mernild et al., 2016c). Precipitation differences observed between the western and eastern sides of the Andes Cordillera occur due to the combination of orographic effects of the mountain relief and the dominating westerly wind direction which results in precipitation amounts and humidity being lower on the eastern Cordillera slopes (Cornwell et al., 2016; Mernild et al., 2016b).

For the central Andes, mean surface air temperatures are normally highest between December and March and lowest in July and August (Masiokas et al., 2016) and temperatures in the Andes showed increasing trends from 1975 to 2006 (~0.25 °C/decade) (Falvey and Garreaud, 2009). The 0 °C isotherm for the western side of the cordillera (40 km northeast of Santiago de Chile), was located at 3385 m a.s.l. between 2009 and 2014 (Mernild et al., 2016c).

3. Data

3.1. MODIS data

The MOD10A1 C6 (henceforth MOD10A1 unless other version is implied) snow product is derived from daily data acquisitions by the MODIS sensor aboard the Terra spacecraft (Riggs et al., 2017). The MODIS global daily snow cover product MOD10A1 (MODIS/Terra Snow Cover Daily L3 Global 500 m Grid) is derived from cloud free observations and is well suited for regional snow cover and albedo mapping (Hall et al., 2002; Liang et al., 2005; Dozier et al., 2008; Rittger et al., 2013; Fausto et al., 2015; Mernild et al., 2015b). The latest MOD10A1 product was released in the spring of 2016 and includes a range of improvements to the previous version including, amongst others, the removal of Terra sensor degradation issues and improvements in atmospheric calibration (Lyapustin et al., 2014). Importantly, the algorithms used to compile the MOD10A1 snow product are modified to include only the best quality observations from the atmospherically corrected MOD10GA product (Hall et al., 2002). Individual MOD10A1 product parts include NDSI, NDSI snow cover (SCE), SAL and corresponding quality control flags. The MOD10A1 NDSI SCE is produced by using an empirical relationship with NDSI values, where NDSI values are multiplied by a constant (Dozier et al., 2008; Hall and Riggs, 2016). By using only full snow cover pixels, the accuracy of the MOD10A1 SAL product is improved in terms of ground truth comparisons (Sorman et al., 2007; Mernild et al., 2015b). The overall error of the MOD10A1 SAL product can vary substantially but is

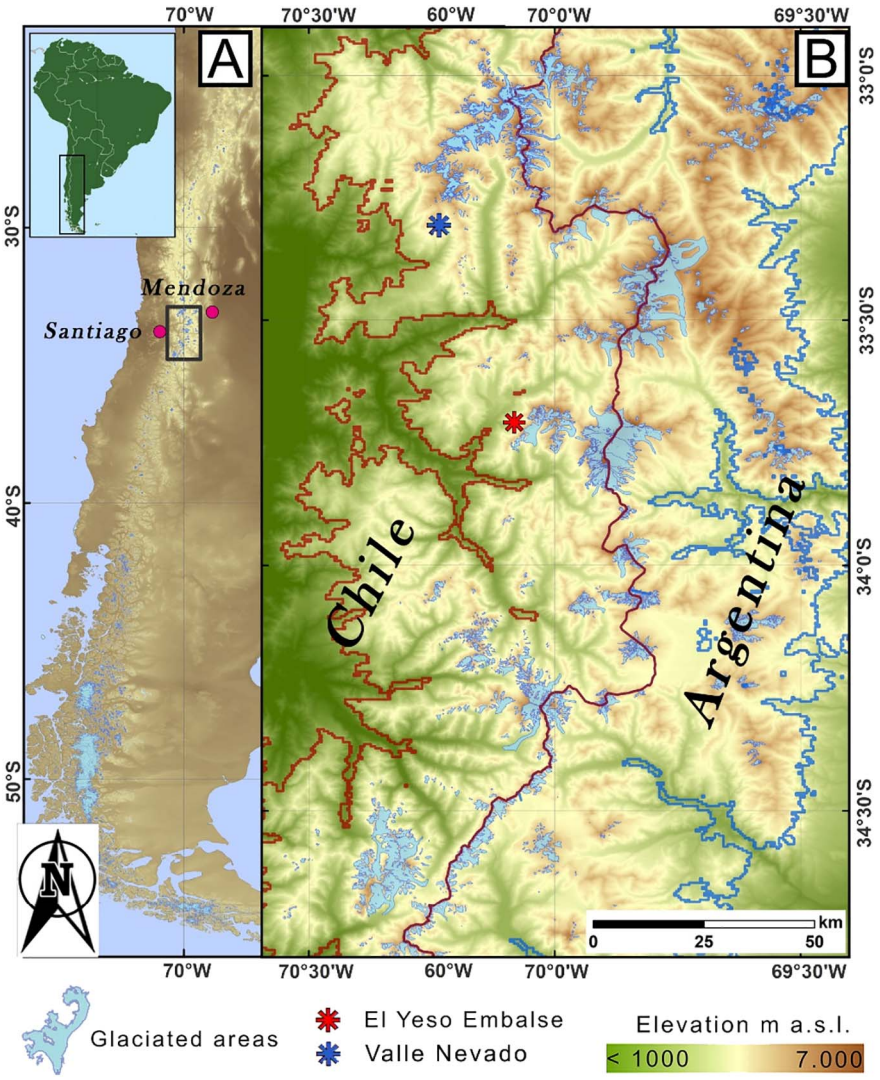

Fig. 1. (a) The central Andes of Chile and Argentina; and (b) including the area of interest west and east snow cover regions delineated by red and blue lines, respectively. The divide between the western and eastern Andes also represents the natural border (continental divide) between Chile and Argentina. Blue areas represent glaciers. The red star in the center of the study area represents the location of the El Yeso Embalse (EYE) meteorological station (2475 m a.s.l.) and the blue star the Valle Nevado (VN) meteorological station (3050 m a.s.l.). (For interpretation of the references to color in this figure legend, the reader is referred to the web version of this article.)

in the order of 1–10% for good observations with low atmospheric disturbances across the Greenland ice sheet (Klein and Stroeve, 2002). The overall error at this location is likely higher due to the complex terrain of the Andes Mountains. However, changes in albedo can still be quantified and here we opted for a per-pixel temporal change analysis that is expected to mitigate the influence of topography to some degree by avoiding direct inter-comparison of pixels influenced by different slope/aspect.

MOD10A1 data used in this study was obtained from the NASA Earth Observation System Data and Information System (EOSDIS) Reverb ECHO website (https://reverb.echo.nasa.gov/). Out of the 5844 potential scenes available between March 1, 2000 and Feb 29, 2016, only 121 (~2%) were missing in the archive, with a maximum temporal gap of 17 days. The snow cover year (season) was set to start 1 March and end February 28 (29) based on analysis of the data set. Pixels with cloud cover or poor retrievals were omitted as determined from QA flags and only pixels flagged as "best quality" were included in the further analysis (see Section 4.1). Out of all pixels in the data series 74.8% contained "best quality" data (Supplementary material S1).

3.2. Ancillary data

Elevation data were obtained from the Shuttle Radar Topography Mission (SRTM) v.3. SRTM provides elevation data at a spatial resolution of 30 m with an overall vertical accuracy of ~10 m and geo-position error of ~9 m (Farr et al., 2007). Multivariate El Niño index (MEI) ranks were obtained from the National Oceanic and Atmospheric Administration (NOAA) website (http://www.esrl.noaa.gov/psd/enso/mei/table.html). The MEI provides a ranked index of the strength of El Niño and La Nina events. MEI values are normalized for each bi-monthly season (Wolter and Timlin, 2011) and cover the 16-year study period of snow cover and snow albedo observations.

We acquired mean monthly air temperature (MMAT), mean annual air temperature (MAAT), and monthly precipitation sums (2000–2016) from the El Yeso Embalse meteorological station (EYE) supported by available data from the Valle Nevado (VN) meteorological station from 2013 onwards (locations in Fig. 1; data shown in Supplementary material S2 and S3) from Dirección General de Aguas (DGA; www.dga.cl) and CryoNET respectively (http://globalcryospherewatch.org/cryonet/sitepage.php?surveyid=68). Finally, glacier outlines were obtained from the Randolph glacier inventory v. 5.0 (Pfeffer et al., 2014) in combination with updated glacier shapes from 2013/2014 (Malmros

Table 1
Input parameters for use in TIMESAT.

Parameter	NDSI snow cover	Snow albedo
Seasonal parameter	0.7	0.7
Number of envelope iterations	3	3
Adaptation strength	2	2
Savitzky-Golay window size	15	15
Spike method	Median filter	Median filter
Amplitude season start (%)	70	65
Amplitude season end (%)	20	46

et al., 2016).

4. Methods

4.1. Time series preprocessing

The MOD10A1 time series was preprocessed and analyzed using the program TIMESAT (Jönsson and Eklundh, 2002, 2004; Eklundh and Jönsson, 2015). TIMESAT originally developed to analyze vegetation seasonality can be applied to all remote sensing data containing seasonal variability. We applied a Savitzky-Golay filter within TIMESAT to smooth the MOD10A1 time-series by applying polynomial fitting to the data points within a moving window of a certain width (Savitzky and Golay, 1964; Jönsson and Eklundh, 2004). Missing dates were filled with blank scenes before smoothing (Jönsson and Eklundh, 2002) in order to compose a complete time series. Pixels not flagged as "best

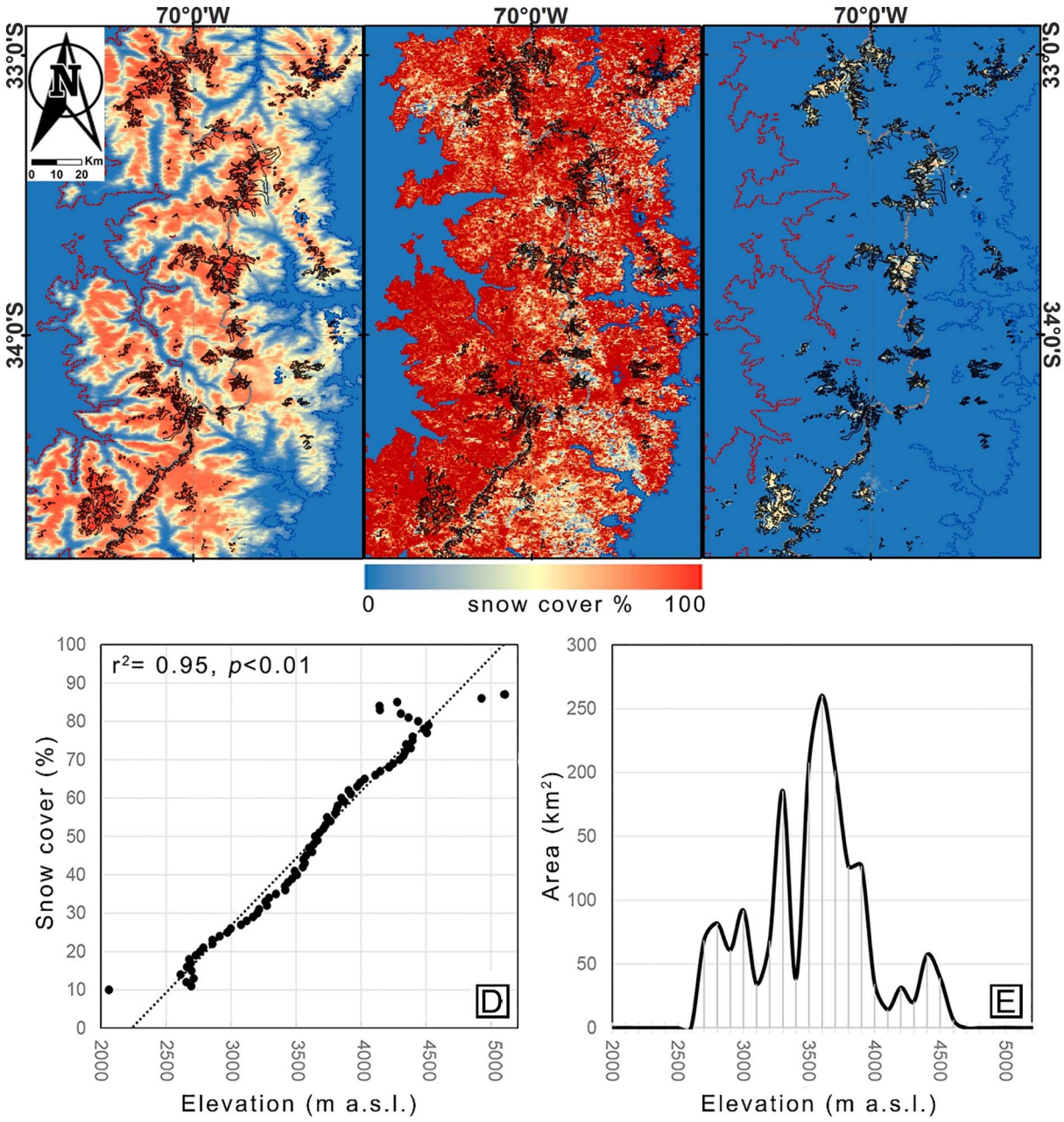

Fig. 2. a) Median snow extent; b) maximum snow cover extent; c) minimum snow cover extent for the 16 snow seasons observed (2000–2016) (glaciers are delineated by black); d) mean SCE change with elevation; and e) snow covered area distribution with elevation.

quality" from the MOD10A1 QA flags were excluded from the analysis. The width of the moving window influences the degree of smoothing and the ability of the filter to cope with rapid changes (parameters used in the TIMESAT preprocessing are shown in Table 1). The polynomial fitting was iterated and adapted to the upper part of the curve by assigning weights to data points above and below the result of the previous step (Jönsson and Eklundh, 2004). SCD was extracted in TIMESAT for SCE, and the seasonal snow cover integral (SCI) (defined as the integral under the curve between onset and end of seasonal snow cover) was extracted to evaluate the accumulated seasonal SCE for each season. Areas characterized by limited seasonal variability were masked out due to the inability of the TIMESAT algorithm to estimate SCD for such conditions. The mask was created from the median of the 16 seasons and excluded areas with < 16 days in the SCD dataset. Most excluded areas were located in glacier accumulation zones where constant snow cover prevents seasonal variability in SCE.

4.2. Trend estimation

We conducted linear temporal trend analysis to estimate the magnitude and direction of changes in SCE, SAL, SCD, SCI, MAAT, and annual precipitation. We calculated per-pixel trends by applying a nonparametric linear regression model with time as the independent variable and the abovementioned variables as dependent variables. Since time series of the variables analyzed often do not meet parametric assumptions of normality and homoscedasticity, a median trend (Theil–Sen, TS) procedure was applied using the Theil-Sen slope estimator (median trend) which has proven robust against outliers (Eastman, 2009). Uncertainty estimates of trends are calculated from standard deviations of the calculated metrics and are provided as ± values to all trends reported. The significance of the trends was determined using the nonparametric Mann–Kendall test of significance (Mann, 1945; Kendall, 1975). The Mann–Kendall significance test is commonly used as a trend test for the TS median slope operator (Eastman, 2009) and produces outputs of z-scores that allow for the assessment of both the significance and direction of trends. The trends were considered significant at $p < 0.05$ (where p denotes the probability that there is no significant difference between observations over time). Trends in SCE, SCD, and SCI were extracted from the area of maximum values (minimum of 75% at any given time) for the entire study period and similar for SAL.

5. Results

5.1. Spatio-temporal patterns in snow cover extent

Statistical analysis of the MODIS time series revealed that the minimum, median, and maximum SCE for the entire observation period and area (Fig. 2) was 2%, 43%, and 74%, respectively. SCE showed the presence of a clear linear relationship with elevation (coefficient of determination (r^2) = 0.95, $p < 0.01$; Fig. 2d). However, the relationship was imperfect ($r^2 = 0.34$) above 4000 m a.s.l. due to increased scattering in the accumulation zone of the glaciers. At its maximum, SCE covered 1730 km^2 (74%) of the study area, only being present at elevations above 1250 m a.s.l. SCE area was normally distributed with highest consentration of SCE observed between 3250 and 4000 m a.s.l. (Fig. 2e). SCE was on average ~11% less on the eastern side of the Cordillera compared to the west (Fig. 2a–c).

5.2. Inter- and intra-annual variability in snow cover extent (SCE) and snow albedo (SAL)

The mean SCE over the study area between 2000 and 2016 was approximately ~25% in austral summer and ~68% in austral winter, reaching a maximum between July 24th and 25th October and a minimum in autumn between March 6th and June 6th (Fig. 3). Overall, spatial trends for SCE and SAL showed widespread downward tendencies (Fig. 4). For SCE, downward trends dominated, with medium SCE decreasing by 13.4 ± 4.0% between 2000 and 2016 (0.35% yr^{-1}). Demonstrating spatial variabilities, the downward trends in SCE were found to be more pronounced for the the eastern side of the Cordillera (13.9 ± 4.0%, 0.9% yr^{-1}) compared to the west (12.4 ± 3.1%, 0.8% yr^{-1}). The eastern side of the Cordillera also showed lower SCE but higher SCE variability compared to the western side, this despite the eastern side being more elevated (mean elevation for the western and eastern sides is 3115 m a.s.l and 3720 m a.s.l, respectively) (Fig. 2d). Median SAL trends from March 2000 to Feburary 2016 were also downward with mean values decreasing by 7.4 ± 2.2% (0.5% yr^{-1}). Downward trends in SAL were shown to be more widespread in the southern parts of the study area compared to northern parts. However, we found no significant differences between the eastern and western sides of the Cordillera.

Comparisons with SRTM data, the SAL trends observed showed negative correlations below ~4600 m a.s.l. (−1.1 ± 0.8% yr^{-1}, r = 0.84, $p < 0.01$). Above ~4600 m a.s.l., however, a distinct shift is observed, with increasing correlations as a function of elevation (0.2 ± 0.01% yr^{-1}, r = 0.83, $p < 0.01$) (Fig. 5). In regards to intra-annual variability, SCE showed pronounced downward trends (< −1% yr^{-1}) during the onset (April, May, and June) and offset (October, November, December, and January) of the snowy season. In comparison to SCE, SAL showed slightly less intra-annual variability with most downward trends occurring during the onset of the snowy season (Fig. 6).

5.3. Snow cover duration (SCD) and seasonal snow cover integral (SCI)

The seasonal SCD values ranged between 0 and 280 days and the seasonal mean SCD ranged between 203 days in the 2005–2006 to 130 days in 2011–2012, with an overall median of 173 days (Fig. 7a). We observed a strong correlation between SCD and elevation (excluding glacier areas). SCD, for example was shown to increase by an average of ~6 days for every 100-meter increment within the 2000 to 4600 m a.s.l. elevation range ($r^2 = 0.80$, $p < 0.01$) (Fig. 7a). Overall, the trends in SCD were downward, showing a mean reduction of 43 ± 20 days for the study period (−2.7 ± 1.3 days yr^{-1}) (Fig. 8a). Trends were especially negative on the eastern side of the Cordillera, with a reduction of 52 ± 36 days (3.3 ± 2.3 days yr^{-1}), whereas on the western side SCD reduced by 35 ± 33 days (2.2 ± 2.0 days yr^{-1}).

The SCI for the entire study area declined by 1.5 ± 0.5% yr^{-1} (median trend), corresponding to 25 ± 8% during the full period of 16 snow seasons. The SCI also shows substantial inter-annual variation (Fig. 9), especially on the eastern side of the Cordillera, where SCI is on average 17% smaller and trends are substantially more downward (1.8 ± 0.5% yr^{-1}) than for the western side (1.2 ± 0.4% yr^{-1}).

5.4. Impact of changes in temperature, precipitation, and El Niño Southern Oscillation (ENSO) on snow cover duration and snow albedo

Analysis of the meteorological data available from the EYE AWS (Fig. 1b) revealed a significant downward trend in precipitation of −4 mm yr^{-1} and an insignificant trend in MAAT of 0.05 °C yr^{-1} between 2000 and 2016. Between 2000 and 2009, nine extreme precipitation events (> 200 mm $month^{-1}$) were identified, with the 2003–2004 season (March–February) receiving a maximum of 1259 mm. These "extreme" events occurred mostly during austral winters and account for large differences in inter-annual precipitation amounts, SCE and SCD sums. Post 2009, no extreme precipitation events occurred, however a minimum of 317 mm was observed for the 2014–2015 season. The mean annual precipitation sum for the 2000 to 2016 observation period was 677 mm. MAAT for this observation period was 9.0 °C, with maximum and minimum values of 10.3 °C and 7.3 °C measured for the 2003–2004 and 2011–2012 seasons,

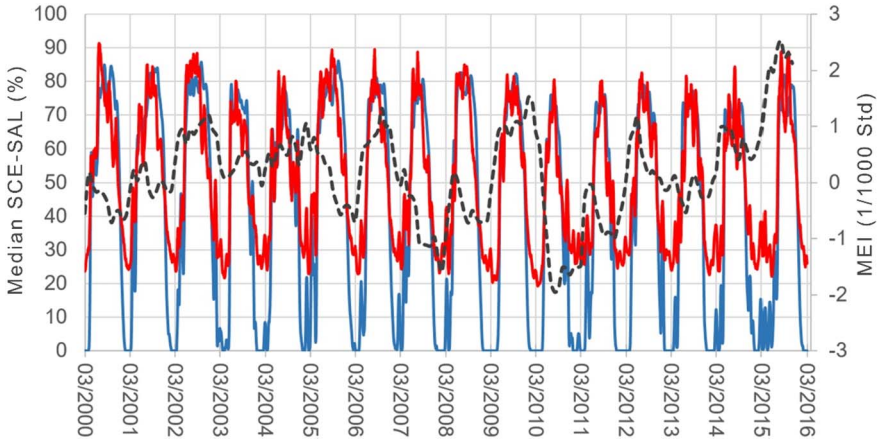

Fig. 3. Variation in daily median SCE (blue) and median SAL (red) percentage and the bi-monthly multivariate ENSO index (MEI) (dark dashed line) in 1/1000 standard variations (Wolter and Timlin, 2011). (For interpretation of the references to color in this figure legend, the reader is referred to the web version of this article.)

respectively.

Statistical comparisons between the MODIS-derived snow data and the observed EYE meteorological data revealed that monthly SCE and SAL averaged over the study area and for the pixel where EYE is located (in brackets) correlated strongly with MMAT (r^2-values of 0.74 (0.71) and 0.82 (0.61), respectively) (Fig. 10a–b). For the VN met-station, the corresponding comparison between SCE and MMAT also show a significant correlation for the 2013 to 2016 period (r^2-values of 0.62). Mean monthly SCE and SAL also correlate with monthly precipitation sums, but to a lesser extent (r^2-values of 0.20 (0.21) and 0.28 (0.19)) (Fig. 10c–d). In comparison, SCI correlated more strongly with annual precipitation sums (r^2-value of 0.84) (Fig. 10e).

There can be large uncertainties introduced by comparing a single station with observations from a larger study area. However, currently it remains the only long-term continuous dataset available in the area, and trends from the local pixel and the station confirms the relationship with trends for the area in general (Fig. 10). Furthermore, EYE and NV temperature data significantly correlated (r^2 of 0.89) showing the temperature trends at EYE and NV being similar at least for that part of the western side of the cordillera in the 2013–2016 period.

ENSO events (MEI) (plotted in Fig. 3) show significant correlations with mean SCE and SAL values for the study area (Fig. 11). Mean correlation coefficient values (r) between MEI and SCE/SAL were strongest when a lag of one month (L1) was applied to the SCE/SAL time series (mean r-values of 0.21 for the study area). Generally, glaciated areas where snow cover is already present are characterized by

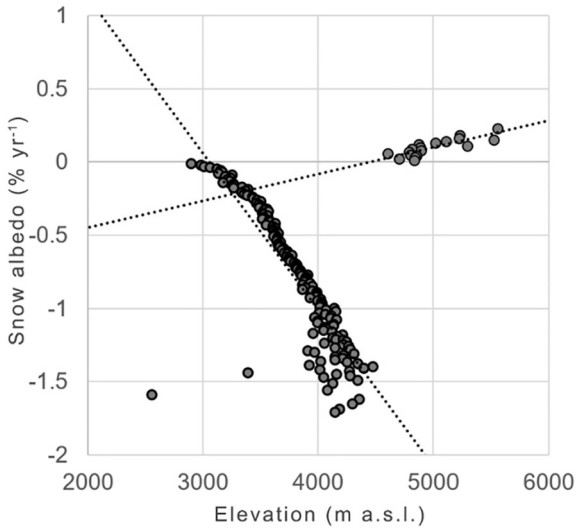

Fig. 5. Trends in snow albedo (SAL) with elevation.

negative SCE and ENSO correlations for shorter lag periods (L1), which is in contrast to the surrounding snow covered areas. This pattern is reversed for longer lag periods (e.g., five months), when glaciated and higher elevated areas significantly correlate with ENSO, whereas surrounding lower altitude areas are characterized by negative

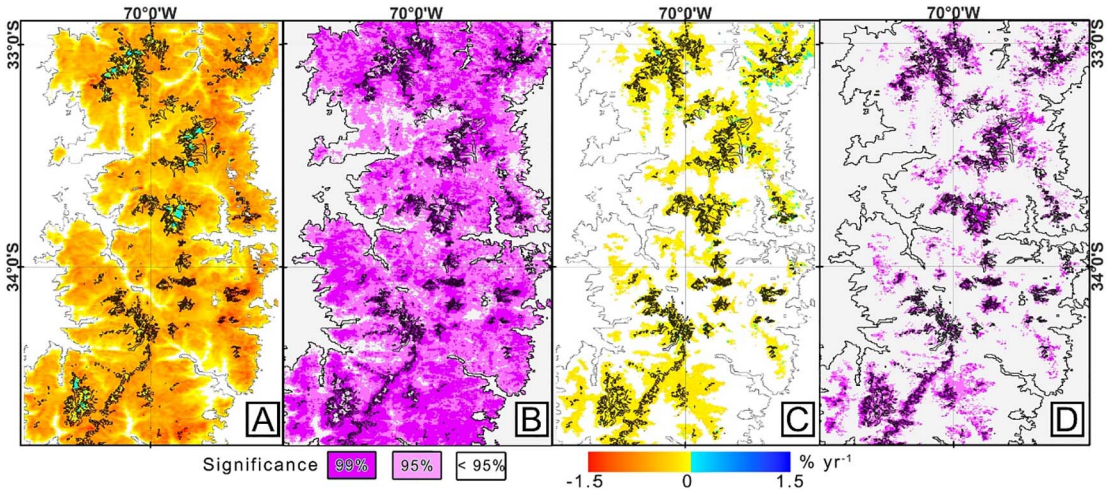

Fig. 4. Linear median trend ($p < 0.05$) in: SCE (a) and SAL (c) from Mar 2000 through Feb 2016, and the corresponding significance level of each trend (b, d).

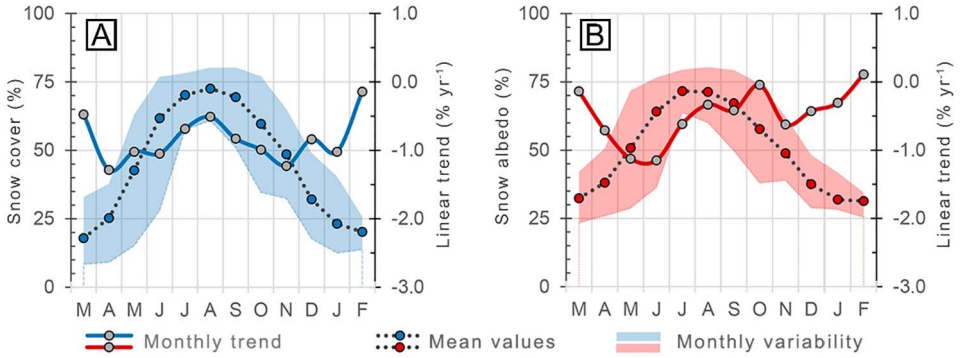

Fig. 6. Intra-annual linear trends (blue and red lines), monthly mean values (dotted lines) and spread (colored areas; monthly minimum and maximum values) in: (a) snow cover extent (SCE); and (b) snow albedo (SAL) between 2000 and 2016. (For interpretation of the references to color in this figure legend, the reader is referred to the web version of this article.)

correlations.

6. Discussion

6.1. Monitoring and assessment of snow cover and snow albedo

Spatio-temporal analysis of MODIS-derived SCE, SAL, SCD, and SCI data revealed significant changes during the observation period of this study. Key to the interpretation of these results is the quantification of sensor related errors and their influence on the trends observed (2000–2016). Unfortunately, only a few validation studies of the MOD10A1 C6 products have been published to date. Recent studies using MOD10A1 collection C6 for the Greenland ice sheet however found that v.C6 corrects for the C5 temporal trend bias in dry snow areas and that albedo retrieval accuracy in C6 is substantially improved over C5 (Box et al., 2017; Casey et al., 2017). Therefore, the accuracy of this product is expected to be better than or at least as good as the C5 product, which has been evaluated in several previous studies (Tekeli et al., 2005; Hall and Riggs, 2007; Gao et al., 2010; Arsenault et al., 2014; Marchane et al., 2015). These studies estimate an overall detection error ranging from ~5% to ~48%, depending on locational properties and type of "ground truth" observations used. In general,

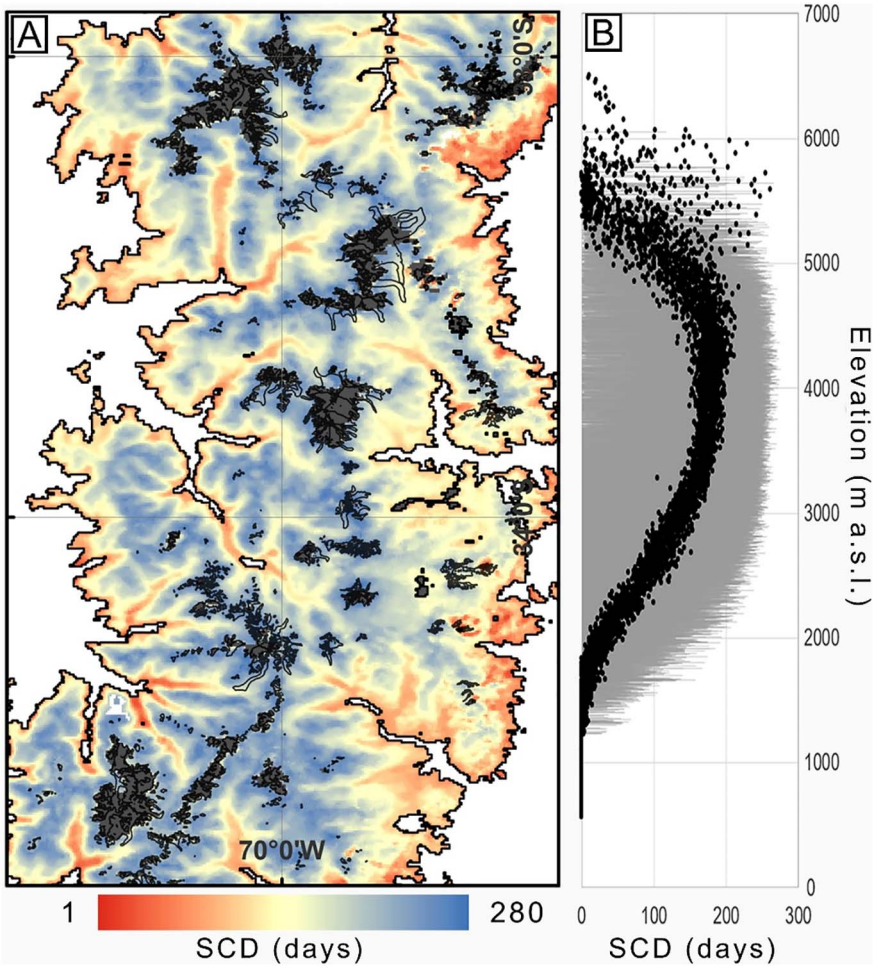

Fig. 7. a) Median snow cover duration (SCD, days) 2000–2016 (dark grey areas represent locations where the model failed to determine seasonality); and (b) mean snow cover duration with elevation for the 2000–2016 period (grey bars show the spread between minimum and maximum values of SCD as a function of elevation).

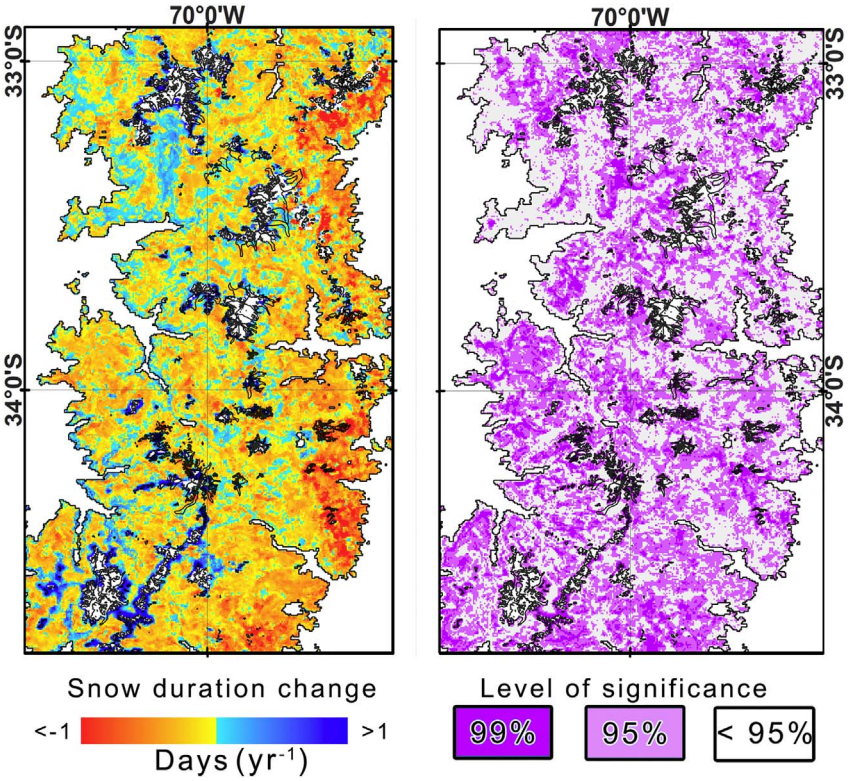

Fig. 8. (a) Per pixel yearly snow cover duration (SCD) trend 2000–2016, and (b) corresponding significance of trend. Dark grey masked areas represent the mask where SCD values are erroneous and black lines represent glaciers.

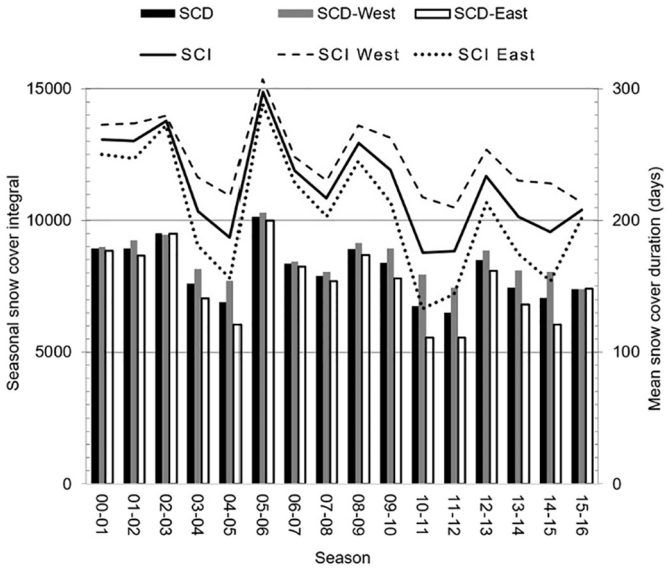

Fig. 9. Mean snow cover duration (SCD, bars) and seasonal snow cover integral (SCI, lines) for the entire study area and for the western (SCD-W) and eastern (SCD-E) sides of the cordillera separately.

spatially homogeneous locations with flat terrain produces less error than in complex terrain with mixed surface as being the case for this study (Wang et al., 2014; Burakowski et al., 2015; Moustafa et al., 2017). By applying a per-pixel temporal change analysis approach in the current study, thereby avoiding direct inter-comparison of pixels characterized by different slope/aspect, the influence of topography is expected to be reduced to some degree. This should also be seen in the context of the latitudinal location of the study area (32°50′–34°5050′ S), characterized by an annual range in solar zenith angles of 28–60 for MODIS overpass times. This makes the region less prone to influences from mountain shadowing as compared to complex terrain of higher latitudes of the northern/southern hemisphere. Snow detection in v.6 is expected to show improvements in comparison to previous versions especially above 1.300 m a.s.l., where the surface temperature screen used in the product algorithm (which has previously caused false negatives) has been rolled back leaving fewer gaps in the data (Hall and Riggs, 2016).

The smoothed and gap-filled MOD10A1 C6 dataset produced with TIMESAT is assumed to correctly represent the seasonal snow distribution for the area. Here, only the best quality MOD10A1 C6 observations (by including information available from the QA flags; 0 = “best quality”) were used for the Savitzky-Golay function fitting in TIMESAT. By adjusting the data fitting to the upper envelope of the daily observations, we ensured that the SCE and SAL values follow rapid changes, which can occur in snow cover extent and albedo. The TIMESAT model uses local function fitting, where values before and after in the time series are considered. This local function fitting reduces the chance of error occurrence in the MOD10A1 observed snow cover (Tekeli et al., 2005). For the upper ablation zones of glaciers, characterized by limited seasonal variability or year round snow SCE, it is not possible to accurately assess seasonality variables and thereby SCD. In this case, a glacier mask was applied based on SCE seasonal variability, in doing so, restricting the SCD analysis to non-glaciated areas (Fig. 7a). Out of 709,029,144 individual pixel records in the time series 24.2% were filled with modeled TIMESAT data.

Snow albedo detection in mountainous environments from remotely sensed imagery can contain large errors when measured on terrain with steep slopes. Validation of satellite or aerial imagery based data using stationary point albedometers can also be challenging because of pronounced mixed pixel and geolocation issues (Liang et al., 2005; Sorman et al., 2007; Mernild et al., 2015b; Box et al., 2017). However, these issues are not likely to have significantly influenced the trends observed in this study as the MOD10A1 pixels are measured in the same pixel

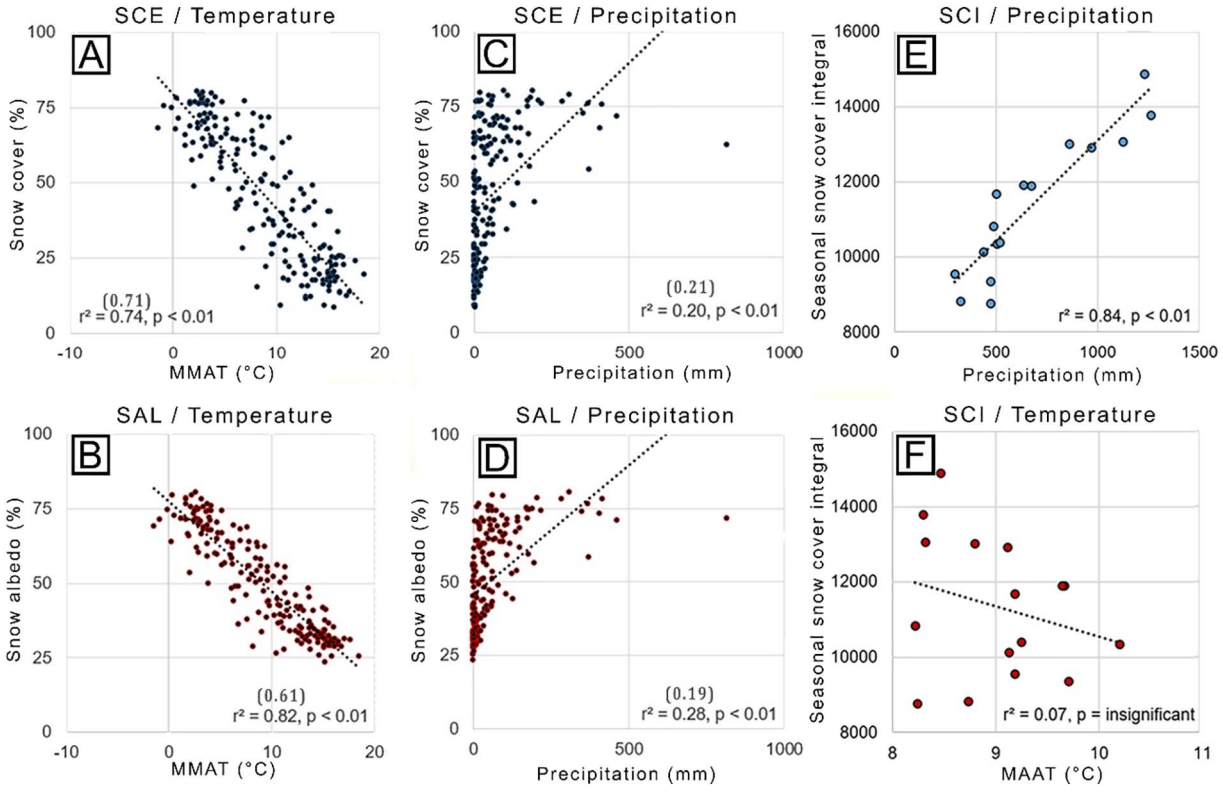

Fig. 10. Relationships between monthly meteorological data (EYE station; Fig. 1) and monthly SCE, monthly SAL, and SCI averaged over the study area. a) Monthly SCE against MMAT; b) monthly SAL against MMAT, c) monthly SCE against monthly precipitation sums, d) monthly SCE against monthly precipitation sums, e) SCI against annual precipitation sums, and f) SCI against MAAT. r^2-Values between the EYE station data and the pixel where it is located is shown in brackets.

location from year to year in a location where seasonal variation in solar zenith angle influence is relatively low (annual range between 28 and 60°) compared to higher latitudes of the northern/southern hemisphere. MOD10A1 snow albedo is produced only for cloud free pixels with full snow cover (+50%) indicating that for pixels characterized by limited full snow cover observations seasonal fitting could have influenced the accuracy of the TIMESAT generated data.

6.2. Analysis of climate variables

The analysis of the effect of local scale climatic variability presented in this study made use of two AWS's EYE and VN in the study area. Indeed, the use of a single or just two AWS's is not ideal when comparing measurements with the spatially large-scale MOD10A1 dataset. Furthermore, given the location of the AWS's on the western side of the cordillera and the presence of distinct climatic gradients (e.g. Mernild et al., 2016a), the data recorded is unlikely to be fully representative of the study area as a whole. However, this scarce coverage of ground

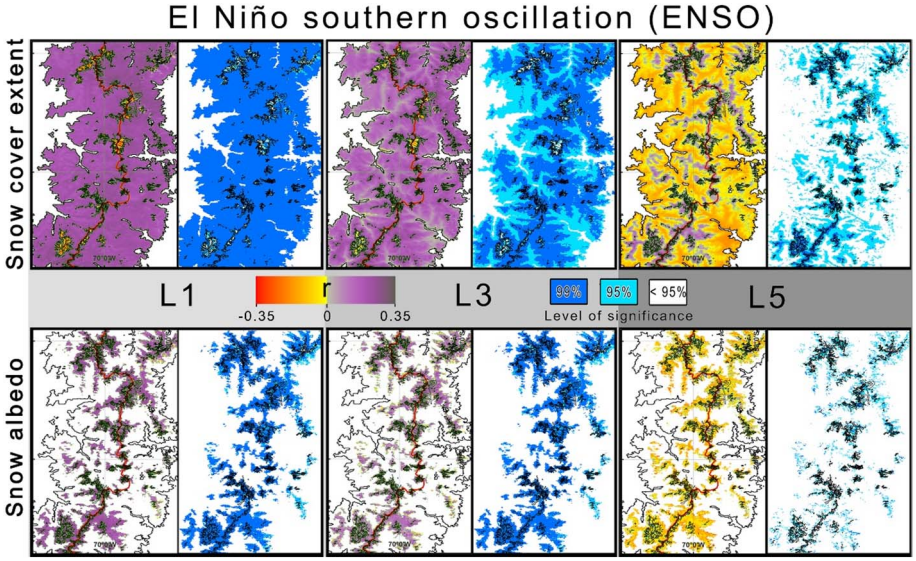

Fig. 11. Per-pixel correlations and significance of SCE/SAL with the ENSO index (MEI) including one-, three- and five-month lag time (L1, L3, and L5). Red line demarks the east west divide. (For interpretation of the references to color in this figure legend, the reader is referred to the web version of this article.)

observations reflects the general conditions for mountainous areas of the Andes and underlines the need for remotely sensed monitoring methods. Additionally, there is a need for high-resolution gridded meteorological products that work well in complex terrain. A high-resolution meteorological dynamical model combined with remote sensing derived products is likely to improve our understanding of the climatic variability impact on snow cover dynamics. Upward trends in MAAT have higher impact the lower the altitudes (mostly noticeable in the southern part of the study area) causing changes in onset and offset of snow seasons to be more sensitive to even small changes in temperature (Fig. 4). Low areas with small slope gradient show higher sensitivity to upward changes in MAAT in regards to snow accumulation. Especially the low elevated areas on the eastern side of the cordillera show the effect of increased MAAT.

Above 4600 m a.s.l., SCD shows a considerable increase in variability (Fig. 7b). This however is not surprising as, in highly elevated zones where SCD can be dependent on localized terrain (slope and area of topographical shadow) and weather conditions. High wind speeds, for example, often make it less likely for snow cover to persist in certain areas despite high levels of solid precipitation.

6.3. Drivers of change on snow cover variables

Studies based on modeling, field measurements and remote sensing have provided insights into the past, current, and future impacts of climate change on snow conditions and runoff in the Andean river catchments of central Chile and Argentina (Pellicciotti et al., 2007; Apaloo et al., 2012; Delbart et al., 2015; Mernild et al., 2015a, 2016a, 2016c; Ragettli et al., 2016). A number of these studies have predicted that air temperatures in the central Andes will continue to increase. An increase in air temperature, together with seasonal changes in precipitation patterns, will likely result in a decrease in the amount of runoff from snow melt and an increase in the amount of runoff from rain (Cai et al., 2014; Mernild et al., 2016a, 2016c; Ragettli et al., 2016). Since the 1970's, precipitation events have generally become more intense but less frequent in central Chile (Falvey and Garreaud, 2007; Garreaud et al., 2009). The EYE precipitation data, for example, shows a number of intense precipitation events (above 200 mm m^{-1}) during the 2000–2009 period. Interestingly, none of these “intense” events occurred during the 2010–2016 period.

Per-pixel correlations between SCE/SAL and the Multivariate El Niño index (MEI) show that MEI has a strong and significant impact on inter-annual SCE/SAL variability in the region (Fig. 11). Although El Niño events are often associated with increases in precipitation, they can also be associated with increases in air temperature (Cai et al., 2014) which, together, can have a pronounced altitude dependent effect on snow cover during spring and autumn. An increase in air temperature, for example, causes the 0 °C isotherm to ascend to higher elevations resulting in a larger proportion of precipitation falling as rain as opposed to snow. Mernild et al. (2016c) observed this phenomenon for the Olivares basin (33°12′ S; 70°09′ W) between 1979 and 2014, where precipitation has been increasingly falling as rain in recent years. This change in the partitioning of precipitation over mountainous areas can offset the positive effects of increased precipitation on snow accumulation, with rainfall often enhancing snow and ice melt rates on glacier surfaces. The significant spatial variation in correlation between MEI and SCE for one-month lag, we suspect is caused by the presence of snow cover on glaciers giving negative or no correlation on short term but increasing correlations with time.

Reduction in SCE in this study has also been studied in modeling studies based on MERRA satellite data (Mernild et al., 2016b, 2016c) which estimate that snow cover extent in the central Andes has reduced ~1.3% per decade 2000–2014 (linear trend, for the b1 window in Fig. 1) (Mernild et al., 2016b). Mernild et al. (2016c) suggest that the largest decreases in snow cover have occurred within the 3000–5000 m a.s.l. elevation range, where > 70% of seasonal precipitation falls as snow. In comparison, the rate of SCE change observed in this study for the same period and area is significantly higher, with per decade reductions equating to ~2.8%. This difference between the results presented here and in Mernild et al. (2016c) may either be an indicator of faster SCE reduction during the 2000–2016 period or highlight possible SCE overestimations in the MERRA model utilized by the latter. For other regions of the world snow cover reductions are well documented. In the Arctic, for example, a general decease in the amount of snow has been observed between 1999 and 2009, together with reductions in maximum winter snow water equivalent, a later snow-cover onset in autumn and earlier snow-free date in spring, and a decreasing snow-cover duration (Liston and Hiemstra, 2011). Indeed a warming trend especially during autumn has been identified at EYE (Burger et al., 2018) and corresponds well with the later onset of snow seasons seen in the area (Fig. 6).

To sustain all year runoff, rivers of the central Andes rely on substantial contributions from snow and ice-melt, and river discharge here is strongly linked to snow cover changes (Delbart et al., 2015). Decreases in SCE at the magnitudes shown in this study has the potential to cause a substantial redistribution in seasonal runoff for this region, where ~21% of river runoff originates from snow- and ice-melt (increasing to ~85% during dry summers) (Peña and Nazarala, 1987; Mernild et al., 2016a). Glaciers in the central Andes are shrinking and down wasting as a consequence of climate warming and changes in precipitation patterns (Masiokas et al., 2006; Bodin et al., 2010; Gacitua et al., 2015; Malmros et al., 2016). Although initially increasing, ice melt runoff will begin to reduce in the future as lowest elevation land ice disappears. If these ice/snow cover trends continue, runoff conditions will likely change, especially during spring, dry summers and periods of drought, affecting the future sustainability of freshwater resources in areas downstream of the central Andes (Peña and Nazarala, 1987; Delbart et al., 2015; Saavedra et al., 2016; Carey et al., 2017; López-Moreno et al., 2017). Whether this change in runoff will cause the low lying areas in the catchment to become wetter or drier is largely determined by local topography (Polk et al., 2017; López-Moreno et al., 2017).

Directly influencing the surface energy balance, the downward trends in SAL revealed in this study (Fig. 4) may possibly result in positive feedbacks in regards to snow and ice melt. This trend of darkening surfaces, either from reduced snow cover or from enhanced melt conditions, is likely to be reinforced by increasing air temperatures and decreasing precipitation (e.g., Mernild et al., 2016c). Another positive feedback could be initiated by the accumulation of dust and debris on glacier surfaces leading to more energy being absorbed and further melt conditions, especially on lower parts of glaciers (Hansen and Nazarenko, 2004; Oerlemans et al., 2009; Arenson et al., 2015). Minimum glacier-wide albedo has shown to be a good predictor for glacier mass balances conditions for temperate glaciers (Dumont et al., 2012; Sirguey et al., 2016; López-Moreno et al., 2017; Polk et al., 2017), which suggests that glaciers in the study area may have positive mass balances, at least for some of the years analyzed. Decreases in surface albedo have also been observed for many other glaciated parts of the world (Box et al., 2012; Tedesco et al., 2013; Abermann et al., 2014; Fausto et al., 2015; Mernild et al., 2015b). The mean albedo for the Greenland ice sheet ablation area (June–August), for example, declined by 22.9% from 2000 to 2016 while dry snow areas only decreased by 1.2% (Box et al., 2017). Increasing albedo values seen above 4.600 m a.s.l. (Fig. 5) are likely contributed to by the increase in precipitation and the presence of dry snow conditions at high altitudes (Box et al., 2017).

The central Andes are dominated by two distinctly different climate systems. On the western side of the Cordillera the climate is influenced by oceanic atmospheric interactions, whereas on the eastern side the climate can be considered continental in type (Prohaska, 1976). This difference in climate is highlighted in this study by the relatively weak correlation between SCE/SAL and MEI on the eastern side of the

Cordillera compared to the west. A higher inter-annual variability in SCE and SCI and more downward trend on the eastern part may be contributed to continental climate conditions (Fig. 9) as also observed in Saavedra et al. (2017).

7. Conclusions and outlook

Overall, snow cover extent (SCE) and snow albedo (SAL) decreased by 13.4 ± 4% and 7.4 ± 2%, respectively, between 2000 and 2016. SCE showed more downward trends on the eastern side of the Andes Cordillera (13.9 ± 4%), while SAL showed a uniform decline thrughout the area. A seasonal analysis revealed downward trends in SCE and SAL for all months of the year, with the largest decreases occuring during the onset (for SCE and SAL) and at the end of the snow seasons (for SCE) ($> 1\%\ yr^{-1}$). SCE showed a near linear increase with elevation ($r^2 = 0.96$, $p < 0.01$), and largest relative losses occuring at elevations above 4.600 m a.s.l. outside glaciated areas. Spatial anaysis of the SAL data revealed increasingly downward trends up to ~4600 m a.s.l. in elevation. Above ~4600 m a.s.l. this trend is reversed, likely because of permanent or semi-permanent dry snow conditions present in glacier accumulation zone. Snow cover duration (SCD) decreased on average by 43 ± 20 days throughout the study area between 2000 and 2016 with largest changes occuring at elevations below 4.500 m a.s.l. on the eastern side and 3.500 m a.s.l. on the western side.

TIMESAT was unable to extract SCD for glacier areas that were covered with snow for most of the year due to the lack of seasonal variation. Additionally, in situations of large variations in snow conditions occuring over a very short time period the Savitzky-Golay seasonal fitting process applied may introduce some errors. SCD trends for the study area indicate a shortening of the snow season between 2000 and 2016. SCI trends for the included glacial areas were also shown to be downward during this 16-year observation period (these being more pronounced on the eastern side of the Cordillera).

The impact of ENSO events, which influence largescale precipitation and temperature patterns in the study area, on the SCE, SCD, and SAL was shown to be evident. Per-pixel analyses revealed that ENSO positively influences SCE/SAL values most strongly with a one-month timelag. Data available from the EYE meteorological station, between 2000 and 2016, reveals that the monthly SCE and SAL values are primarliy determined by variations in temperature, while montly SCI values are determined mostly by precipitation. If the observed decline in SCE persist in the coming years, it will likely result in a a seasonal redistribution of avaliable downstream freshwater which may cause future problems for people and agriculture in the region.

Supplementary data to this article can be found online at https://doi.org/10.1016/j.rse.2018.02.072.

Acknowledgements

We extend a special thanks to the editor and the reviewers for their insightful critique of this article. This work was supported by the Chilean Fondecyt Regular Competition under grant agreement #1140172. All data requests should be addressed to the first author. The authors have no conflict of interest.

References

Abermann, J., Kinnard, C., MacDonell, S., 2014. Albedo variations and the impact of clouds on glaciers in the Chilean semi-arid Andes. J. Glaciol. 60, 183–191.
Apaloo, J., Brenning, A., Bodin, X., 2012. Interactions between seasonal snow cover, ground surface temperature and topography (Andes of Santiago, Chile, 33.5°S). Permafr. Periglac. Process. 23, 277–291.
Arenson, L.U., Jakob, M., Wainstein, P., 2015. Effects of dust deposition on glacier ablation and runoff at the Pascua-Lama Mining Project, Chile and Argentina. In: Lollino, G., Manconi, A., Clague, J., Shan, W., Chiarle, M. (Eds.), Engineering Geology for Society and Territory. Climate Change and Engineering Geology, vol. 1. Springer International Publishing, Cham, pp. 27–32.
Arsenault, K.R., Houser, P.R., De Lannoy, G.J.M., 2014. Evaluation of the MODIS snow cover fraction product. Hydrol. Process. 28, 980–998.
Benn, D.I., Evans, D.J.A., 2010. Glaciers and Glaciation. Hodder Education, London.
Bodin, X., Rojas, F., Brenning, A., 2010. Status and evolution of the cryosphere in the Andes of Santiago (Chile, 33.5 degrees S). Geomorphology 118, 453–464.
Box, J.E., Fettweis, X., Stroeve, J.C., Tedesco, M., Hall, D.K., Steffen, K., 2012. Greenland ice sheet albedo feedback: thermodynamics and atmospheric drivers. Cryosphere 6, 821–839.
Box, J.E., Van As, D., Steffen, K., Fausto, R.S., Ahlstrøm, A.P., Citterio, M., Andersen, S.B., 2017. Greenland, Canadian and Icelandic land-ice albedo grids (2000–2016). Geol. Surv. Den. Greenl. Bull. 38, 53–56.
Brock, B.W., Willis, I.C., Sharp, M.J., 2000. Measurement and parameterization of albedo variations at Haut Glacier d'Arolla, Switzerland. J. Glaciol. 46, 675–688.
Burakowski, E.A., Ollinger, S.V., Lepine, L., Schaaf, C.B., Wang, Z., Dibb, J.E., Hollinger, D.Y., Kim, J., Erb, A., Martin, M., 2015. Spatial scaling of reflectance and surface albedo over a mixed-use, temperate forest landscape during snow-covered periods. Remote Sens. Environ. 158, 465–477.
Burger, F., Brock, B., Montecinos, A., 2018. Seasonaland elevational contrasts in temperature trends in Central Chile between 1979 and 2015. Glob. Planet. Chang. 162, 136–147.
Cai, W., Borlace, S., Lengaigne, M., van Rensch, P., Collins, M., Vecchi, G., Timmermann, A., Santoso, A., McPhaden, M.J., Wu, L., England, M.H., Wang, G., Guilyardi, E., Jin, F.-F., 2014. Increasing frequency of extreme El Nino events due to greenhouse warming. Nat. Clim. Chang. 4, 111–116.
Carey, M., Molden, O.C., Rasmussen, M.B., Jackson, M., Nolin, A.W., Mark, B.G., 2017. Impacts of glacier recession and declining meltwater on mountain societies. Ann. Am. Assoc. Geogr. 107, 350–359.
Casey, K.A., Polashenski, C.M., Chen, J., Tedesco, M., 2017. Impact of MODIS sensor calibration updates on Greenland Ice Sheet surface reflectance and albedo trends. Cryosphere 11, 1781–1795.
Cereceda-Balic, F., Palomo-Marín, M.R., Bernalte, E., Vidal, V., Christie, J., Fadic, X., Guevara, J.L., Miro, C., Pinilla Gil, E., 2012. Impact of Santiago de Chile urban atmospheric pollution on anthropogenic trace elements enrichment in snow precipitation at Cerro Colorado, Central Andes. Atmos. Environ. 47, 51–57.
Cornwell, E., Molotch, N.P., McPhee, J., 2016. Spatio-temporal variability of snow water equivalent in the extra-tropical Andes Cordillera from distributed energy balance modeling and remotely sensed snow cover. Hydrol. Earth Syst. Sci. 20, 411–430.
Corripio, J.G., Purves, R.S., 2006. Surface energy balance of high altitude glaciers in the Central Andes: the effect of snow penitentes. In: Climate and Hydrology in Mountain Areas. John Wiley & Sons, Ltd, pp. 15–27.
Cuffey, K.M., Paterson, W.S.B., 2010. The Physics of Glaciers. Elsevier Science.
Dariane, A.B., Khoramian, A., Santi, E., 2017. Investigating spatiotemporal snow cover variability via cloud-free MODIS snow cover product in Central Alborz Region. Remote Sens. Environ. 202, 152–165.
Delbart, N., Dunesme, S., Lavie, E., Madelin, M., Goma, R., 2015. Remote sensing of Andean mountain snow cover to forecast water discharge of Cuyo rivers. J. Alp. Res. 15.
Dozier, J., Frew, J., 1981. Atmospheric corrections to satellite radiometric data over rugged terrain. Remote Sens. Environ. 11, 191–205.
Dozier, J., Painter, T.H., Rittger, K., Frew, J.E., 2008. Time-space continuity of daily maps of fractional snow cover and albedo from MODIS. Adv. Water Resour. 31, 1515–1526.
Dubayah, R., 1992. Estimating net solar-radiation using Landsat thematic mapper and digital elevation data. Water Resour. Res. 28, 2469–2484.
Dumont, M., Gardelle, J., Sirguey, P., Guillot, A., Six, D., Rabatel, A., Arnaud, Y., 2012. Linking glacier annual mass balance and glacier albedo retrieved from MODIS data. Cryosphere 6, 1527–1539.
Eastman, J.R., 2009. IDRISI Taiga Guide to GIS and Image Processing. Clark Labs Clark University, Worcester, MA.
Eklundh, L., Jönsson, P., 2015. TIMESAT: a software package for time-series processing and assessment of vegetation dynamics. In: Kuenzer, C., Dech, S., Wagner, W. (Eds.), Remote Sensing Time Series: Revealing Land Surface Dynamics. Springer International Publishing, Cham, pp. 141–158.
Escobar, F., Casassa, G., Pozo, V., 1995. Variaciones de un glaciar de Montaña en los Andes de Chile Central en las últimas dos décadas. Bull. Inst. Fr. Etudes Andines 24, 683–995.
Falvey, M., Garreaud, R., 2007. Wintertime precipitation episodes in Central Chile: associated meteorological conditions and orographic influences. J. Hydrometeorol. 8, 171–193.
Falvey, M., Garreaud, R.D., 2009. Regional cooling in a warming world: recent temperature trends in the southeast Pacific and along the west coast of subtropical South America (1979–2006). J. Geophys. Res.-Atmos. 114.
Farr, T.G., Rosen, P.A., Caro, E., Crippen, R., Duren, R., Hensley, S., Kobrick, M., Paller, M., Rodriguez, E., Roth, L., Seal, D., Shaffer, S., Shimada, J., Umland, J., Werner, M., Oskin, M., Burbank, D., Alsdorf, D., 2007. The shuttle radar topography mission. Rev. Geophys. 45 (n/a-n/a).
Fausto, R.S., van As, D., Antoft, J.A., Box, J.E., Colgan, W., Team, P.P., 2015. Greenland ice sheet melt area from MODIS (2000–2014). In: Geological Survey of Denmark and Greenland Bulletin, pp. 57–60.
Gacitua, G., Uribe, J.A., Wilson, R., Loriaux, T., Hernandez, J., Rivera, A., 2015. 50 MHz helicopter-borne radar data for determination of glacier thermal regime in the central Chilean Andes. Ann. Glaciol. 56.
Gao, Y., Xie, H.J., Yao, T.D., Xue, C.S., 2010. Integrated assessment on multi-temporal and multi-sensor combinations for reducing cloud obscuration of MODIS snow cover products of the Pacific Northwest USA. Remote Sens. Environ. 114, 1662–1675.
Gardner, A.S., Sharp, M.J., 2010. A review of snow and ice albedo and the development of a new physically based broadband albedo parameterization. J. Geophys. Res. Earth Surf. 115.

Garreaud, R.D., Vuille, M., Compagnucci, R., Marengo, J., 2009. Present-day South American climate. Palaeogeogr. Palaeoclimatol. Palaeoecol. 281, 180–195.
Gurung, D.R., Maharjan, S.B., Shrestha, A.B., Shrestha, M.S., Bajracharya, S.R., Murthy, M.S.R., 2017. Climate and topographic controls on snow cover dynamics in the Hindu Kush Himalaya. Int. J. Climatol. 37, 3873–3882.
Hall, D.K., Riggs, G.A., 2007. Accuracy assessment of the MODIS snow products. Hydrol. Process. 21, 1534–1547.
Hall, D.H., Riggs, G., 2016. In: National Snow and Ice Data Center (NSIDC) (Ed.), MODIS/Terra Snow Cover Daily L3 Global 500 m Grid, Version 6. NASA, Boulder, Colorado USA.
Hall, D.K., Riggs, G.A., Salomonson, V.V., 1995. Development of methods for mapping global snow cover using moderate resolution imaging spectroradiometer data. Remote Sens. Environ. 54, 127–140.
Hall, D.K., Riggs, G.A., Salomonson, V.V., DiGirolamo, N.E., Bayr, K.J., 2002. MODIS snow-cover products. Remote Sens. Environ. 83, 181–194.
Hansen, J., Nazarenko, L., 2004. Soot climate forcing via snow and ice albedos. Proc. Natl. Acad. Sci. U. S. A. 101, 423–428.
Hock, R., 2005. Glacier melt: a review of processes and their modelling. Prog. Phys. Geogr. 29, 362–391.
Huang, X., Deng, J., Wang, W., Feng, Q., Liang, T., 2017. Impact of climate and elevation on snow cover using integrated remote sensing snow products in Tibetan Plateau. Remote Sens. Environ. 190, 274–288.
Jönsson, P., Eklundh, L., 2002. Seasonality extraction by function fitting to time-series of satellite sensor data. IEEE Trans. Geosci. Remote Sens. 40, 1824–1832.
Jönsson, P., Eklundh, L., 2004. TIMESAT - a program for analyzing time-series of satellite sensor data. Comput. Geosci. 30, 833–845.
Justice, C.O., Vermote, E., Townshend, J.R.G., Defries, R., Roy, D.P., Hall, D.K., Salomonson, V.V., Privette, J.L., Riggs, G., Strahler, A., Lucht, W., Myneni, R.B., Knyazikhin, Y., Running, S.W., Nemani, R.R., Wan, Z.M., Huete, A.R., van Leeuwen, W., Wolfe, R.E., Giglio, L., Muller, J.P., Lewis, P., Barnsley, M.J., 1998. The Moderate Resolution Imaging Spectroradiometer (MODIS): land remote sensing for global change research. IEEE Trans. Geosci. Remote Sens. 36, 1228–1249.
Kendall, M.G., 1975. Rank Correlation Methods. Griffin, London.
Klein, A.G., Stroeve, J., 2002. Development and validation of a snow albedo algorithm for the MODIS instrument. Ann. Glaciol. 34, 45–52.
Knap, W.H., Brock, B.W., Oerlemans, J., Willis, I.C., 1999. Comparison of Landsat TM-derived and ground-based albedos of Haut Glacier d'Arolla, Switzerland. Int. J. Remote Sens. 20, 3293–3310.
Konzelmann, T., Ohmura, A., 1995. Radiative fluxes and their impact on the energy-balance of the Greenland ice-sheet. J. Glaciol. 41, 490–502.
Leiva, J.C., 1999. Recent fluctuations of the Argentinian glaciers. Glob. Planet. Chang. 22, 169–177.
Li, C., Su, F., Yang, D., Tong, K., Meng, F., Kan, B., 2017a. Spatiotemporal variation of snow cover over the Tibetan Plateau based on MODIS snow product, 2001–2014. Int. J. Climatol. http://dx.doi.org/10.1002/joc.5204.
Li, X., Fu, W., Shen, H., Huang, C., Zhang, L., 2017b. Monitoring snow cover variability (2000–2014) in the Hengduan Mountains based on cloud-removed MODIS products with an adaptive spatio-temporal weighted method. J. Hydrol. 551, 314–327.
Liang, S.L., Stroeve, J., Box, J.E., 2005. Mapping daily snow/ice shortwave broadband albedo from Moderate Resolution Imaging Spectroradiometer (MODIS): the improved direct retrieval algorithm and validation with Greenland in situ measurement. J. Geophys. Res.-Atmos. 110.
Liston, G.E., Hiemstra, C.A., 2011. The changing cryosphere: pan-Arctic snow trends (1979–2009). J. Clim. 24, 5691–5712.
López-Moreno, J.I., Valero-Garcés, B., Mark, B., Condom, T., Revuelto, J., Azorín-Molina, C., Bazo, J., Frugone, M., Vicente-Serrano, S.M., Alejo-Cochachin, J., 2017. Hydrological and depositional processes associated with recent glacier recession in Yanamarey catchment, Cordillera Blanca (Peru). Sci. Total Environ. 579, 272–282.
Lyapustin, A., Wang, Y., Xiong, X., Meister, G., Platnick, S., Levy, R., Franz, B., Korkin, S., Hilker, T., Tucker, J., Hall, F., Sellers, P., Wu, A., Angal, A., 2014. Scientific impact of MODIS C5 calibration degradation and C6+ improvements. Atmos. Meas. Tech. 7, 4353–4365.
Male, D.H., Granger, R.J., 1981. Snow surface-energy exchange. Water Resour. Res. 17, 609–627.
Malmros, J.K., Mernild, S.H., Wilson, R., Yde, J.C., Fensholt, R., 2016. Glacier area changes in the central Chilean and Argentinean Andes 1955–2013/14. J. Glaciol. 62, 391–401.
Mann, H.B., 1945. Nonparametric tests against trend. Econometrica 13, 245–259.
Marchane, A., Jarlan, L., Hanich, L., Boudhar, A., Gascoin, S., Tavernier, A., Filali, N., Le Page, M., Hagolle, O., Berjamy, B., 2015. Assessment of daily MODIS snow cover products to monitor snow cover dynamics over the Moroccan Atlas mountain range. Remote Sens. Environ. 160, 72–86.
Masiokas, M.H., Villalba, R., Luckman, B.H., Le Quesne, C., Aravena, J.C., 2006. Snowpack variations in the central Andes of Argentina and Chile, 1951–2005: large-scale atmospheric influences and implications for water resources in the region. J. Clim. 19, 6334–6352.
Masiokas, M.H., Christie, D.A., Le Quesne, C., Pitte, P., Ruiz, L., Villalba, R., Luckman, B.H., Berthier, E., Nussbaumer, S.U., González-Reyes, Á., McPhee, J., Barcaza, G., 2016. Reconstructing the annual mass balance of the Echaurren Norte glacier (Central Andes, 33.5° S) using local and regional hydroclimatic data. Cryosphere 10, 927–940.
McClung, D.M., 2013. The effects of El Niño and La Niña on snow and avalanche patterns in British Columbia, Canada, and central Chile. J. Glaciol. 59, 783–792.
Mernild, S.H., Liston, G.G., Kane, D.L., Knudsen, N.F., Hasholt, B., 2008. Snow, runoff, and mass balance modeling for the entire Mittivakkat Glacier (1998–2006), Ammassalik Island, SE Greenland. Geogr. Tidsskr. Dan. J. Geogr. 108, 121–136.
Mernild, S.H., Beckerman, A.P., Yde, J.C., Hanna, E., Malmros, J.K., Wilson, R., Zemp, M., 2015a. Mass loss and imbalance of glaciers along the Andes Cordillera to the sub-Antarctic islands. Glob. Planet. Chang. 133, 109–119.
Mernild, S.H., Malmros, J.K., Yde, J.C., Wilson, R., Knudsen, N.T., Hanna, E., Fausto, R.S., van As, D., 2015b. Albedo decline on Greenland's Mittivakkat Gletscher in a warming climate. Int. J. Climatol. 35, 2294–2307.
Mernild, S.H., Liston, G.E., Hiemstra, C.A., Malmros, J.K., Yde, J.C., McPhee, J., 2016a. The Andes Cordillera. Part I: snow distribution, properties, and trends (1979–2014). Int. J. Climatol. 37 (4), 1680–1698.
Mernild, S.H., Liston, G.E., Hiemstra, C.A., Beckerman, A.P., Yde, J.C., McPhee, J., 2016b. The Andes Cordillera. Part IV: spatiotemporal freshwater runoff distribution to adjacent seas (1979–2014). Int. J. Climatol. 37 (7), 3175–3196.
Mernild, S.H., Liston, G.E., Hiemstra, C.A., Yde, J.C., McPhee, J., Malmros, J.K., 2016c. The Andes Cordillera. Part II: Rio Olivares basin snow conditions (1979–2014), Central Chile. Int. J. Climatol. 37 (4), 1699–1715.
Meza, F.J., Wilks, D.S., Gurovich, L., Bambach, N., 2012. Impacts of climate change on irrigated agriculture in the Maipo Basin, Chile: reliability of water rights and changes in the demand for irrigation. J. Water Resour. Plan. Manag. 138, 421–430.
Montecinos, A., Aceituno, P., 2003. Seasonality of the ENSO-related rainfall variability in central Chile and associated circulation anomalies. J. Clim. 16, 281–296.
Moustafa, S.E., Rennermalm, A.K., Román, M.O., Wang, Z., Schaaf, C.B., Smith, L.C., Koenig, L.S., Erb, A., 2017. Evaluation of satellite remote sensing albedo retrievals over the ablation area of the southwestern Greenland ice sheet. Remote Sens. Environ. 198, 115–125.
Neckel, N., Loibl, D., Rankl, M., 2017. Recent slowdown and thinning of debris-covered glaciers in south-eastern Tibet. Earth Planet. Sci. Lett. 464, 95–102.
Oerlemans, J., Giesen, R.H., Van den Broeke, M.R., 2009. Retreating alpine glaciers: increased melt rates due to accumulation of dust (Vadret da Morteratsch, Switzerland). J. Glaciol. 55, 729–736.
Pellicciotti, F., Burlando, P., Van Vliet, K., 2007. Recent trends in precipitation and streamflow in the Aconcagua River basin, central Chile Glacier mass balance changes and meltwater discharge. In: Foz do Iguaçu. International Association of Hydrological Sciences: IAHS.
Peña, H., Nazarala, B., 1987. Snowmelt-Runoff Simulation Model of a Central Chile Andean Basin with Relevant Orographic Effects. International Association of Hydrological Sciences (IAHS), Vancouver, Canada.
Pfeffer, W.T., Arendt, A.A., Bliss, A., Bolch, T., Cogley, J.G., Gardner, A.S., Hagen, J.-O., Hock, R., Kaser, G., Kienholz, C., Miles, E.S., Moholdt, G., Mölg, N., Paul, F., Radi, Valentina, Rastner, P., Raup, B.H., Rich, J., Sharp, M.J., 2014. The Randolph Glacier Inventory: a globally complete inventory of glaciers. J. Glaciol. 60, 537–552.
Polk, M.H., Young, K.R., Baraer, M., Mark, B.G., McKenzie, J.M., Bury, J., Carey, M., 2017. Exploring hydrologic connections between tropical mountain wetlands and glacier recession in Peru's Cordillera Blanca. Appl. Geogr. 78, 94–103.
Prohaska, F., 1976. The climate of Argentina, Paraguay and Uruguay. In: Schwerdfeger, W. (Ed.), World Survey of Climatology. Elsevier, New York, pp. 13–112.
Ragettli, S., Immerzeel, W.W., Pellicciotti, F., 2016. Contrasting climate change impact on river flows from high-altitude catchments in the Himalayan and Andes Mountains. Proc. Natl. Acad. Sci. U. S. A. 113, 9222–9227.
Riggs, G.A., Hall, D.K., Román, M.O., 2017. Overview of NASA's MODIS and visible infrared imaging radiometer suite (VIIRS) snow-cover earth system data records. Earth Syst. Sci. Data 9, 765–777.
Rittger, K., Painter, T.H., Dozier, J., 2013. Assessment of methods for mapping snow cover from MODIS. Adv. Water Resour. 51, 367–380.
Rutllant, J., Fuenzalida, H., 1991. Synoptic aspects of the Central Chile rainfall variability associated with the Southern Oscillation. Int. J. Climatol. 11, 63–76.
Saavedra, F.A., Kampf, S.K., Fassnacht, S.R., Sibold, J.S., 2016. A snow climatology of the Andes Mountains from MODIS snow cover data. Int. J. Climatol. 37 (3), 1526–1539.
Saavedra, F.A., Kampf, S.K., Fassnacht, S.R., Sibold, J.S., 2017. Changes in Andes Mountains snow cover from MODIS data 2000–2014. Cryosphere Discuss. http://dx.doi.org/10.5194/tc-2017-72. (in review).
Savitzky, A., Golay, M.J.E., 1964. Smoothing and differentiation of data by simplified least squares procedures. Anal. Chem. 36, 1627–1639.
Sirguey, P., Still, H., Cullen, N.J., Dumont, M., Arnaud, Y., Conway, J.P., 2016. Reconstructing the mass balance of Brewster Glacier, New Zealand, using MODIS-derived glacier-wide albedo. Cryosphere 10, 2465–2484.
Sorman, A.U., Akyurek, Z., Sensoy, A., Sorman, A.A., Tekeli, A.E., 2007. Commentary on comparison of MODIS snow cover and albedo products with ground observations over the mountainous terrain of Turkey. Hydrol. Earth Syst. Sci. 11, 1353–1360.
Tedesco, M., Fettweis, X., Mote, T., Wahr, J., Alexander, P., Box, J.E., Wouters, B., 2013. Evidence and analysis of 2012 Greenland records from spaceborne observations, a regional climate model and reanalysis data. Cryosphere 7, 615–630.
Tekeli, A.E., Akyürek, Z., Arda Şorman, A., Şensoy, A., Ünal Şorman, A., 2005. Using MODIS snow cover maps in modeling snowmelt runoff process in the eastern part of Turkey. Remote Sens. Environ. 97, 216–230.
Vuille, M., Kaser, G., Juen, I., 2008. Glacier mass balance variability in the Cordillera Blanca, Peru and its relationship with climate and the large-scale circulation. Glob. Planet. Chang. 62, 14–28.
Wang, Z., Schaaf, C.B., Strahler, A.H., Chopping, M.J., Román, M.O., Shuai, Y., Woodcock, C.E., Hollinger, D.Y., Fitzjarrald, D.R., 2014. Evaluation of MODIS albedo product (MCD43A) over grassland, agriculture and forest surface types during dormant and snow-covered periods. Remote Sens. Environ. 140, 60–77.
Warren, S.G., Wiscombe, W.J., 1980. A model for the spectral albedo of snow. II: snow containing atmospheric aerosols. J. Atmos. Sci. 37, 2734–2745.
Wilson, R., Mernild, S.H., Malmros, J.K., Bravo, C., CarriÓN, D., 2016. Surface velocity fluctuations for Glaciar Universidad, central Chile, between 1967 and 2015. J. Glaciol. 62, 847–860.

Wiscombe, W.J., Warren, S.G., 1980. A model for the spectral albedo of snow. I: pure snow. J. Atmos. Sci. 37, 2712–2733.
Wolter, K., Timlin, M.S., 2011. El Niño/Southern Oscillation behaviour since 1871 as diagnosed in an extended multivariate ENSO index (MEI.ext). Int. J. Climatol. 31, 1074–1087.
Xu, W., Ma, H., Wu, D., Yuan, W., 2017. Assessment of the daily cloud-free MODIS snow-cover product for monitoring the snow-cover phenology over the Qinghai-Tibetan Plateau. Remote Sens. 9, 585.